International Journal of Heat and Mass Transfer 52 (2009) 1827–1842

Contents lists available at ScienceDirect

International Journal of Heat and Mass Transfer

journal homepage: www.elsevier.com/locate/ijhmt

Dispersion of a buoyant plume in a turbulent pressure-driven channel flow

Alexandre Fabregat, Jordi Pallarès *, Ildefonso Cuesta, Francesc Xavier Grau

Departament d'Enginyeria Mecànica, Universitat Rovira i Virgili, Av. Països Catalans, 26, 43007 Tarragona, Spain

ARTICLE INFO

Article history:
Received 14 April 2008
Available online 6 December 2008

Keywords:
DNS
Plane channel flow
Turbulent heat transfer
Buoyancy

ABSTRACT

Direct numerical simulations of the turbulent dispersion of a buoyant line of hot fluid released at the inlet of a plane channel flow are reported ($Re_\tau = 180$, $Gr = 10^7$ and $Pr = 0.7$). Results of turbulent dispersion of a neutrally buoyant scalar and mixed convection flow are also included. The buoyancy force induces a vertical movement that, although small in mean, exhibits a significant fluctuation in the vertical velocity component and deflects the plume with the consequent loss of symmetry found in the neutrally buoyant results. The modification of the budgets for the time averaged momentum and heat transport equations reflects the rearranging of the different contributions induced by the buoyancy force.

1. Introduction

The simulation of the dispersion from concentrated sources is of scientific and technological importance because it has implications, for example, in the prediction of the dispersion of a contaminant released from a smokestack in the atmospheric boundary layer or the mixing of chemical species in chemical reactors.

The early studies carried out by Taylor [1,2], Uberoi and Corrsin [3] and Townsend [4] dealt with scalar dispersion in turbulent homogeneous and isotropic turbulence. Sawford and Hunt [5] developed a Lagrangian stochastic model to predict the effect of molecular diffusion and viscosity on scalar fluctuations in stationary homogeneous turbulence. Their results were compared with the experimental data of Stapountzis et al. [6] demonstrating that molecular diffusion and viscosity affect the development of the thermal plume and particularly the intensity of the temperature fluctuations in all the stages of the plume. This flow was also studied numerically by Anand and Pope [7] using Probability Density Functions (PDF) methods and by Livescu et al. [8] who used Direct Numerical Simulation (DNS) to study the dispersion from line sources in homogeneous isotropic turbulence.

The dispersion of a line source placed in an homogeneous turbulent shear flow was analyzed experimentally by Stapountzis and Britter [9], Karnik and Tavoularis [10] and Chunk and Kyong [11] to determine the effect of the flow anisotropy on the scalar dispersion. These authors reported the mean scalar distributions, the fluctuations intensities and detailed information about the velocity–temperature correlations, the temperature PDFs and the joint velocity–temperature PDFs. Numerical results were reported by Wilson et al. [12] and Cho and Chung [13].

Scalar dispersion in turbulent channel flow is an example of mixing in a non-isotropic turbulent flow. Dispersion from line sources in boundary layers has been considered by Shlien and Corrsin [14]. These authors found that the mean temperature profile downstream the source approached an asymptotic form when it is normalized adequately. Paranthoën et al. [15] deduced a rescaling scheme based on the temporal Lagrangian scale of the vertical velocity fluctuations. This scaling collapses the mean temperature profiles into a single curve. However, it was found that this scaling is not adequate for the temperature fluctuation intensities. Fackrell and Robins [16] measured variance, intermittency, peak concentration values, PDF and spectra of scalar concentration for ground and elevated locations in turbulent boundary layers. These authors reported the contributions of the different terms of the transport equations of the variance and the turbulent fluxes. Additional experimental measurements of the dispersion in turbulent boundary layers can be found in Legg et al. [17] Veeravalli and Warhaft [18], Bara et al. [19], Tong and Warhaft [20] and Vincent et al. [21]. Scalar transport in low-Reynolds-number channel flows was simulated by Lyons et al. [22], Papavassiliou and Hanratty [23] and Na and Hanratty [24]. Kontomaris and Hanratty [25] studied the effects of molecular diffusivity on the dispersion of a passive scalar released from a point source located at the centerline of a turbulent channel flow. Mito and Hanratty [26] studied the dispersion of heat markers released from point sources located at different distances away from wall using a lagrangian approach. Le and Papavassiliou [27] used a similar method to track heat markers released from line sources at different locations away the wall for the channel and Couette flows for a wide range of *Pr* numbers. DNS of dispersion from point sources in fully developed pipe flow has been performed by Brethouwer et al. [28]. Single and double line sources of passive scalars in fully developed channel flows were

* Corresponding author.
E-mail address: jordi.pallares@urv.cat (J. Pallarès).

0017-9310/$ - see front matter © 2008 Elsevier Ltd. All rights reserved.
doi:10.1016/j.ijheatmasstransfer.2008.10.011

Nomenclature

Letters

C_f	friction coefficient
g	gravity acceleration
Gr	Grashof number
H_S	line source half-width
k	turbulent kinetic energy
L_i	domain size in the direction i
Pr	Prandtl number
$Re_{2\delta}$	Reynolds number based on the bulk velocity
Re_τ	Reynolds number based on the friction velocity
T	temperature
u, v, w	streamwise, spanwise and wall-normal velocity components
x, y, z	streamwise, spanwise and wall-normal coordinates

Greek symbols

α	thermal diffusivity
β	volumetric thermal expansion coefficient
δ	channel half-width
δ_{ij}	Kronecker delta
ν	kinematic viscosity
σ_0	line source initial height
τ	shear stress
θ	non-dimensional temperature

Superscripts and subscripts

b	bulk value
$'$	fluctuation
∞	referred to the bulk
$+$	wall coordinates
ref	reference value
H	referred to the hot wall
C	referred to the cold wall
w	referred to a wall
0	referred to the line source

studied by Vrieling and Nieuwstadt [29]. Flows at higher Reynolds numbers and high aspect-ratio channels were studied experimentally by Lavertu and Mydlarski [30]. In other works, the passive scalar was released and absorbed at walls [31] or the scalar fluxes were imposed at the walls [22] providing additional information about the turbulence statistics of temperature. DNS in combination with Lagrangian methods has been used to study forced convection from sources located at the channel walls [32,23]. Experiments of dispersion from line sources of non-reacting passive scalars and reactive scalars have been carried out in homogeneous turbulence [33,34,6]. Other authors performed numerical simulations of dispersion of non-conserved passive scalars released from line sources obtaining information about the influence of the mixing process on the chemical reaction rates [29,35].

Other inhomogeneous turbulent flows including developed channel and turbulent boundary layer flows have been studied by Bernard and Rovelstad [36], Wang and Komori [37] and Iliopoulos and Hanratty [38].

The turbulent pressure-driven channel flow is used in this study as the basic configuration to analyze the coupling between momentum and heat transport by buoyancy effects. The main objective is to study the turbulent heat transport in a horizontal channel from a buoyant plume formed when hot fluid is released within the channel through a vertically centered horizontal line source located at the inlet. To the authors' knowledge this flow configuration has not been previously reported in the literature. This system has implications in applications in which the mixing processes are affected by buoyancy. The turbulent flows considered in this study include:

- Case A: Scalar line source in a channel at $Re_\tau = 180$
- Case B: Mixed convection at $Re_\tau = 150$ and $Gr = 9.6 \times 10^5$
- Case C: Buoyant source line in a channel at $Re_\tau = 180$ and $Gr = 10^7$

Before attempting the simulation of case C, we simulated two flow configurations (cases A and B) for which there are results available in the literature. These two cases, with implications in the dispersion of a buoyant source line in a channel, were used to determine the feasibility of the present simulations of the buoyant source. Case A can be considered as a benchmark to analyze the passive scalar mixing in a non-homogeneous turbulent flow. On the other hand case B considers the buoyancy effects on the turbulent mixing of a scalar, which is a key ingredient in the dispersion of a buoyant line in a channel flow.

2. Physical models

The flow configurations considered in this work are based on the fully developed pressure-driven channel flow between two parallel, infinite and smooth walls placed a distance 2δ apart. The streamwise, spanwise and wall-normal directions are denoted as x, y and z, respectively. A sketch of the domain including the coordinate system is shown in Fig. 1. The origin is indicated in this figure as the point O.

The cases considered are summarized in Table 1, which includes the grid resolution, the Reynolds number based on the friction velocity and the half-width of the channel, the Reynolds number based on the bulk velocity and the width of the channel and the Prandtl and Grashof numbers.

The dimensions of the computational domain for all the cases are $8\pi\delta \times 2\pi\delta \times 2\delta$ in the x, y and z directions, respectively. The two walls of the channel are rigid and immobile. They are located at $z = -\delta$ and $z = \delta$ and are considered adiabatic for cases A and C and at fixed but different temperatures for case B.

2.1. Case A: Temperature line source in a channel at $Re_\tau = 180$

The first flow configuration considered corresponds to a fully developed channel flow where non-buoyant hot fluid is released from a horizontal line source vertically centered at the inlet of the channel (see Fig. 1). In this case, temperature acts as a passive scalar (i.e. $Gr = 0$). At the inlet the source line is implemented as a spanwise band centered in the middle of the channel ($z = 0$) with a

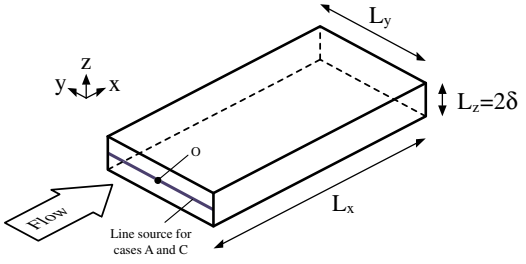

Fig. 1. Sketch of the channel configuration.

Table 1
Summary of flow configurations.

Case	Description	Grid resolution	Re_τ	$Re_{2\delta}$	Gr	Buoyancy	Pr
A	Passive plume	$258 \times 130 \times 130$	180	5452	0	None	0.71
B	Mixed convection	$131 \times 101 \times 101$	150	2722	9.6×10^5	x	0.71
C	Buoyant plume	$258 \times 130 \times 130$	180	5476	10^7	z	0.71

size of $2H_S$ where $H_S = 0.054\delta$. The corresponding temperature distribution is $T(0,y,z,t) = T_0 \forall z \in [-H_S, H_S]$ and $T(0,y,z,t) = T_\infty \forall z \ni [-H_S, H_S]$.

2.2. Case B: Mixed convection at $Re_\tau = 150$ and $Gr = 9.6 \times 10^5$

The configuration for case B corresponds to a mixed convection fully developed flow in a channel with the gravity vector aligned with the streamwise direction. The streamwise and spanwise directions are considered homogeneous and periodic boundary conditions are applied for the velocity, pressure and temperature fields. The temperatures on the bottom and top walls are considered constant and prescribed to be $T(x,y,-\delta,t) = T_H$ and $T(x,y,\delta,t) = T_C$, respectively.

2.3. Case C: Buoyant source line in a channel at $Re_\tau = 180$ and $Gr = 10^7$

Case C is similar to case A in which a horizontal source line is vertically centered at the channel inlet but, as in case B, momentum and heat are coupled through the buoyancy term. However, in case C, the gravity vector is aligned with the z direction, which is normal to the walls of the channel (see Fig. 1 and Table 1). The plume formed by the source line is hotter than the background colder fluid and, due to the density differences, the buoyancy forces tend to deflect the plume towards the top wall.

3. Mathematical models

The non-dimensional equations governing the conservation of momentum and thermal energy for a Newtonian incompressible fluid can be written as:

$$\frac{\partial u_i}{\partial x_i} = 0 \tag{1}$$

$$\frac{\partial u_i}{\partial t} + u_j \frac{\partial u_i}{\partial x_j} = \delta_{i1} - \frac{\partial p'}{\partial x_i} + \frac{1}{Re_\tau} \frac{\partial^2 u_i}{\partial x_j \partial x_j} + \frac{Gr}{8 Re_\tau^2} (\theta - \theta_{ref}) \tag{2}$$

$$\frac{\partial \theta}{\partial t} + u_j \frac{\partial \theta}{\partial x_j} = \frac{1}{Pr Re_\tau} \frac{\partial^2 \theta}{\partial x_j \partial x_j} \tag{3}$$

All the physical properties are assumed to be constant, except for the density in the buoyancy term, which is assumed to be a linear function of temperature according to the Boussinesq approximation [39]. The dimensionless parameters appearing in the Eqs. (2) and (3) are defined as:

$$Re_\tau = \frac{u_\tau \delta}{\nu} \tag{4}$$

$$Pr = \frac{\nu}{\alpha} \tag{5}$$

$$Gr = \frac{\Delta T (2\delta)^3}{\nu^2} g\beta \tag{6}$$

The length and velocity scales used to define the non-dimensional variables are the channel half-width and the averaged friction velocity, respectively. The non-dimensional temperatures are $\theta = \frac{T - T_\infty}{T_o - T_\infty}$, for cases A and C and $\theta = \frac{T - T_C}{T_H - T_C}$ for case B. In Eq. (2) θ_{ref} is the non-dimensional reference temperature. For cases A and C, $T_{ref} = T_\infty (\theta_{ref} = 0)$ and for case B, $T_{ref} = \frac{T_H + T_C}{2} (\theta_{ref} = \frac{1}{2})$. The first term in the right hand side of Eq. (2) is the non-dimensional averaged pressure gradient.

The set of governing equations and boundary conditions has been solved numerically with the finite volume code 3DINAMICS. The Poisson equation resulting from the coupling between the velocity and pressure fields is solved efficiently with a parallel multigrid technique [40]. The momentum equation has been integrated in time using the Crank–Nicholson second-order implicit scheme. A centered second-order finite volume approach has been used to discretize the convective and diffusive terms of the momentum equations. The same temporal and spatial discretization schemes have been used to numerically integrate the heat transport equation in the case B. For cases A and C, the discrete line source implemented at the inlet of the channel has associated large gradients of temperature and the non-linear advective term in the heat transport equation leads to non-physical values for the temperature when the centered second-order finite volume approach is used. To overcome this problem, an Adams–Bashforth second-order explicit time integration has been used for time integration. The Total Variation Diminishing (TVD) scheme [41] has been implemented for the discretization of the advective terms of the thermal energy equation (Eq. 3) in cases A and C.

The grid resolutions used for the simulations are indicated in Table 1. Uniform grid distributions are used along the spanwise and streamwise directions with sizes ($\Delta x^+ = 17.7$, $\Delta y^+ = 8.8$), ($\Delta x^+ = 29.2$, $\Delta y^+ = 9.5$) and ($\Delta x^+ = 17.7$, $\Delta y^+ = 8.8$), for cases A, B and C, respectively. The grid nodes are stretched towards the walls of the channels. The minimum and maximum grid spacings along the wall-normal direction are ($\Delta z^+_{\min} = 0.4$, $\Delta z^+_{\max} = 4.8$), ($\Delta z^+_{\min} = 0.3$, $\Delta z^+_{\max} = 5.5$) and ($\Delta z^+_{\min} = 0.4$, $\Delta z^+_{\max} = 4.8$), for cases A, B and C, respectively.

The spanwise direction is homogeneous for all the variables in the three cases considered and consequently periodic boundary conditions are imposed along this direction. For case A homogeneity along the streamwise direction is considered for the hydrodynamic field but not for the temperature field. At the outlet of the channel non-reflecting boundary conditions are applied for temperature. For case A, interpolated results of an instantaneous flow field of a previous simulation at $Re_\tau = 150$ have been used as initial conditions.

For case B periodic boundary conditions are imposed along the streamwise and spanwise directions. The hydrodynamic variables have been initialized using instantaneous fields of a previous simulation of a fully developed channel flow. The temperature has been initialized with a constant distribution at the reference temperature ($T(x,y,z,0) = T_{ref}$) for which the buoyancy force is zero. It was found that the simulations are very sensitive to the temperature initial conditions. For example, difficulties in achieving steady statistics were experienced when temperature was initialized using a linear profile from the cold to the hot wall. It was also found that for this mixed convection case, a shorter domain along the streamwise direction than that used produced no quasi-steady conditions for the bulk velocity and the bulk temperature, which varied in time with a very low frequency [42].

For case C the dynamic field can not be considered homogeneous along the streamwise direction because of the coupling between momentum and heat equations. To generate realistic boundary conditions at the inlet of the channel where the line source is located, a buffer region has been attached at the inlet of the channel. A sketch of the computational domain including the

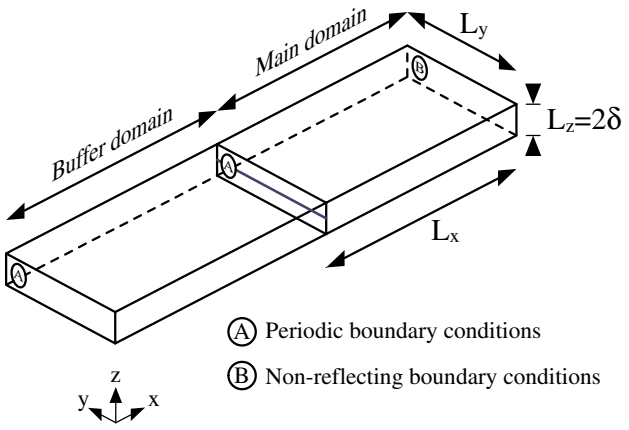

Fig. 2. Buffer domain.

buffer is shown in Fig. 2. The size of the computational domain and the mesh distribution in the buffer region are the same as in the main domain. At each time step the flow in the buffer region is computed and the velocity and pressure distributions at the outlet of the buffer region are used as the boundary conditions for the computation of the flow in the main domain where the plume develops. At the outlet of the channel, non-reflecting boundary conditions are used for velocity, pressure and temperature.

The nondimensional time steps used for time integration are $\Delta t = 5 \times 10^{-4}$ for cases A and C and $\Delta t = 10^{-3}$ for case B. The flow statistics have been averaged when the flows were statistically developed during 60, 200 and 70 non-dimensional time units for cases A, B and C, respectively. Those averaging time periods for cases A and C are respectively about 40 and 45 times larger than the integral time scale of the wall shear stress fluctuations and about 120 and 140 times the integral time scale of the fluctuations of the streamwise velocity component at the centerline of the channel.

4. Results

4.1. Case A: Scalar line source in a channel at $Re_\tau = 180$

Fig. 3 shows the mean velocity profile (Fig. 3a) and the profiles of the fluctuation intensities (Fig. 3b) compared with DNS of a fully developed channel flow at $Re_\tau = 180$ reported by Iwamoto [43]. This author used a grid resolution of $128 \times 128 \times 128$ with a computational domain of sizes $12.8\delta \times 6.4\delta \times 2\delta$ in the streamwise, spanwise and wall-normal directions, respectively. It can be seen that there is a general agreement of the present results with the DNS of Iwamoto [43]. The differences that can be observed in Fig. 3 can be explained by the fact that this author used spectral methods to solve the momentum equations along the homogeneous directions. The Reynolds number based on the channel centerline velocity and the channel half-width and the friction coefficient are $Re_c = 3176$ and $C_f = 0.0084$, in agreement with those reported by Iwamoto [43], ($Re_c = 3245$ and $C_f = 0.0083$).

Fig. 4 shows the comparison between the present predictions of the mean centerline temperature decay (Fig. 4a) and the plume half-width (Fig. 4b) and DNS performed by Brethouwer and Nieuwstadt [35] and Vrieling and Nieuwstadt [29].

Brethouwer and Nieuwstadt [35] simulated the flow field in a fully developed channel with a vertically centered line source at $Re_\tau = 180$ and $Pr = 0.7$ with a grid resolution of $225 \times 120 \times 78$ in a computational domain with sizes $10\delta \times 6\delta \times 2\delta$. They solved the momentum equations in this domain and the scalar transport in a computational box three times larger along the streamwise

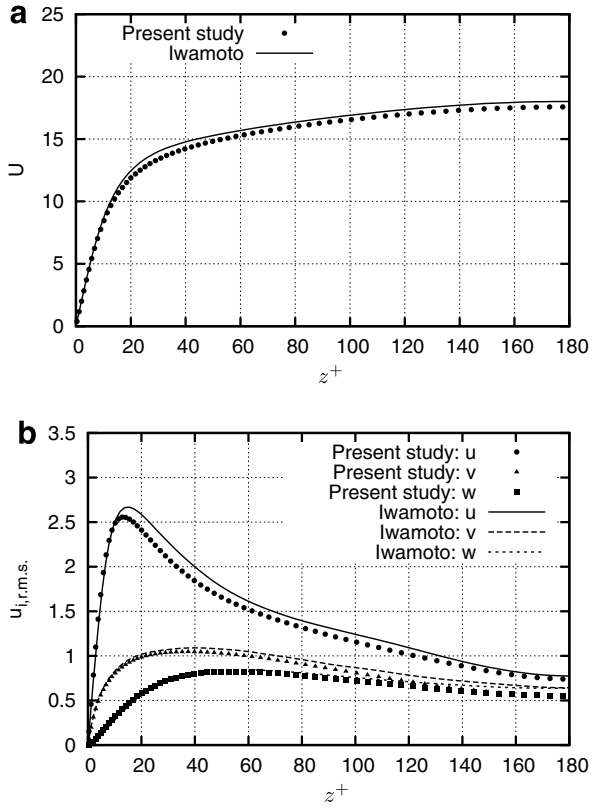

Fig. 3. Mean (a) and r.m.s. (b) velocity profiles.

direction ($30\delta \times 6\delta \times 2\delta$) using the periodic extension of the flow field computed in the smaller domain.

Vrieling and Nieuwstadt [29] used a grid resolution of $150 \times 96 \times 150$ in a computational domain with sizes $10\ \delta \times 6\delta \times 2\delta$ to simulate dispersion and chemical reactions for a vertically centered single source in a fully developed channel at $Re_\tau = 180$ and $Pr = 1.0$.

It is important to note that Brethouwer and Nieuwstadt [35] considered a smaller size for the line source ($H_S = 0.028\delta$) than that used in this study ($H_S = 0.054\delta$). The evolution of the plume decay (Fig. 4a) agrees with that reported by Vrieling and Nieuwstadt [29] who considered a Gaussian line source with an initial width $\sigma_0 = 0.02$. The plume half-width results obtained by Brethouwer and Nieuwstadt [35] are in agreement with those reported in the present study and both differ from those obtained by Vrieling and Nieuwstadt [29] (Fig. 4b). The difference in the definition of the source (gaussian or top-hat) can explain the larger σ values observed. Different grid resolutions and Prandtl numbers may also contribute to these differences between the present results (and those reported by Brethouwer and Nieuwstadt [35]) and those by Vrieling and Nieuwstadt [29].

The mean centerline temperature decay rate for homogeneous turbulence is well described by a power law of the form $\overline{T}/T_0 \propto (x/h)^n$ according to Karnik and Tavoularis [10]. The fit of the present results to this power law, gives a value $n = -0.6$ which is the same than that reported by Lavertu and Mydlarsky [30]. This value is smaller than that obtained for homogeneous turbulence for which $n = -0.75$ to -1.0 for distances $x/M \geqslant 1$ where M is the mesh length of the turbulence-generating grid. These authors suggest that at larger values of x the exponent n should decrease to values of the order of -0.5 [34].

Fig. 5 shows the comparison of the r.m.s. profiles with numerical results of Brethouwer and Nieuwstadt [35] and experiments carried out by Sawford and Sullivan [44]. These authors measured

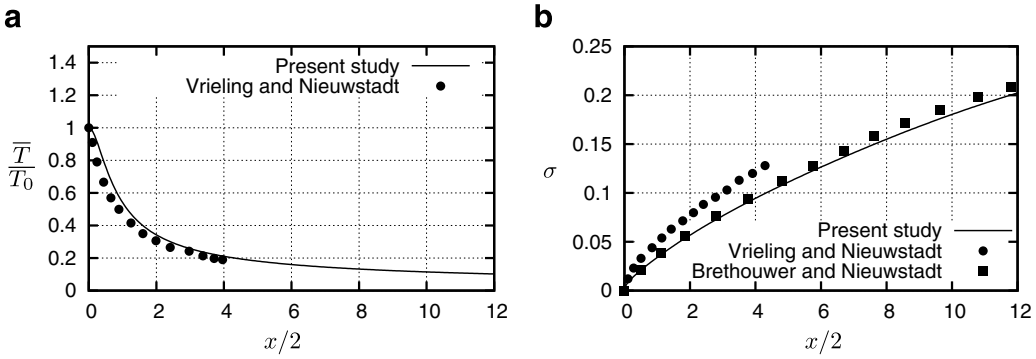

Fig. 4. Mean centerline decay (a) and half-width plume (b) for temperature.

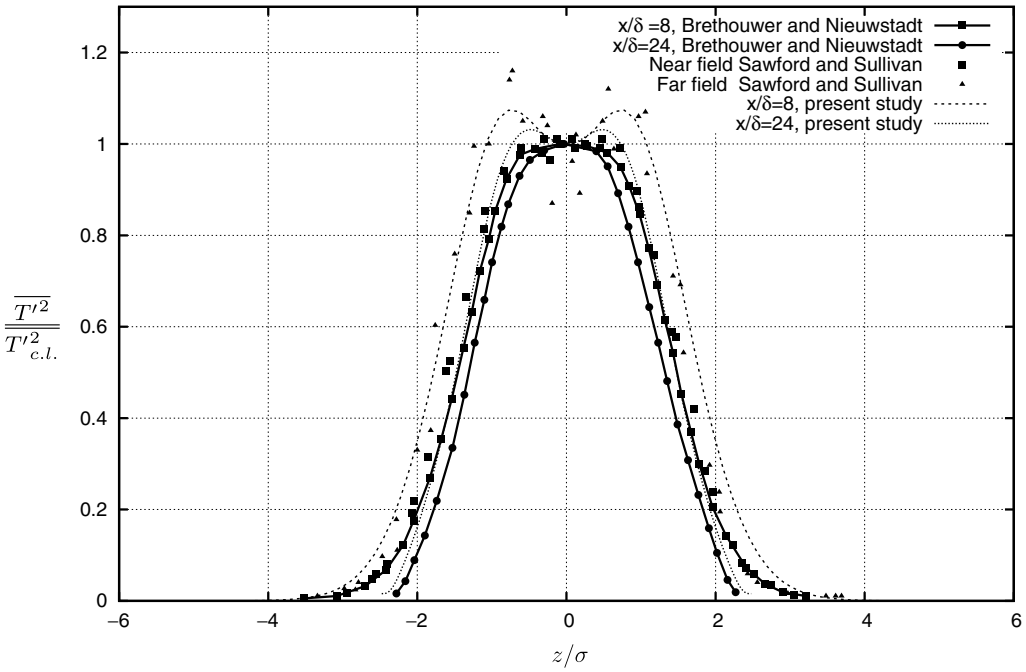

Fig. 5. Temperature r.m.s. profiles.

the dispersion in grid generated turbulence obtaining results for scalar dispersion in homogeneous turbulence. It has been seen that for this type of flows the r.m.s. profile near the source exhibits two off-center peaks. These peaks are not found for mid-field positions but they appear again for further distances in the far field. This re-emergence for the r.m.s. peaks in homogeneous turbulence was explained by Karnik and Tavoularis [10] and it is shown by Sawford and Sullivan [44].

The present results show also these two off-center peaks in the r.m.s. profiles. At $x/\delta = 8$ the intensity of the peaks is larger than at $x/\delta = 24$. This can be explained because of the non-homogeneity of the flow introduced by the walls. The non-homogeneity in wall-normal direction introduced in channel flows tends to exhibit a single peak in the r.m.s. profiles as the distance downstream increases [30]. On the other hand, the reason why Brethouwer and Nieuwstadt [35] r.m.s. profiles do not show peaks can be attributed to the fact that the size of their source is smaller (0.028δ) than that considered in this study (0.054δ).

4.2. Case B: Mixed convection at $Re_\tau = 150$ and $Gr = 9.6 \times 10^5$

The profiles of the mean temperature and the fluctuation intensities are shown in Fig. 6 while the profiles of the mean streamwise velocity and the r.m.s. of the velocity components are shown in Fig. 7.

The results are in agreement with those of available in the literature [45] as shown in Figs. 6 and 7. Some relevant mean quantities are presented in Table 2 where the values reported by Davidson et al. [45] are indicated in parentheses. The largest difference between these values is found in the bulk velocity (7.9%).

It can be seen that the time averaged temperature profile shown in Fig. 6a is not antisymmetric with respect to the channel center $z = 0$. On average, buoyancy acts as a sink for the streamwise momentum equation at $z > -0.6$ and as a source at $z < -0.6$. Consequently the velocity profiles are non-symmetric with respect the channel centerline and the wall shear stresses at the two walls of the channel are different as indicated in Table 2.

The velocity fluctuations are larger near the cold wall as it can be seen in Fig. 7b while the temperature fluctuations are larger near the hot wall (see Fig. 6b). A discussion of this effect can be found in [45].

4.3. Case C: Buoyant source line in a channel at $Re_\tau = 180$ and $Gr = 10^7$

4.3.1. Mean velocity and temperature fields

The mean streamwise velocity is shown in Fig. 8a and in Fig. 8b in wall and δ-scaled coordinates respectively for three selected

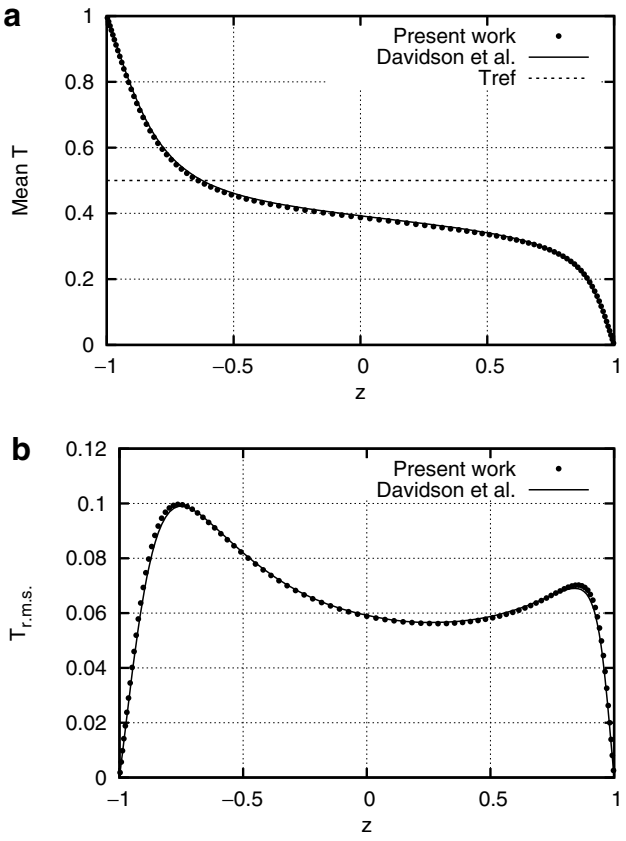

Fig. 6. Mean (a) and r.m.s. (b) temperature profiles.

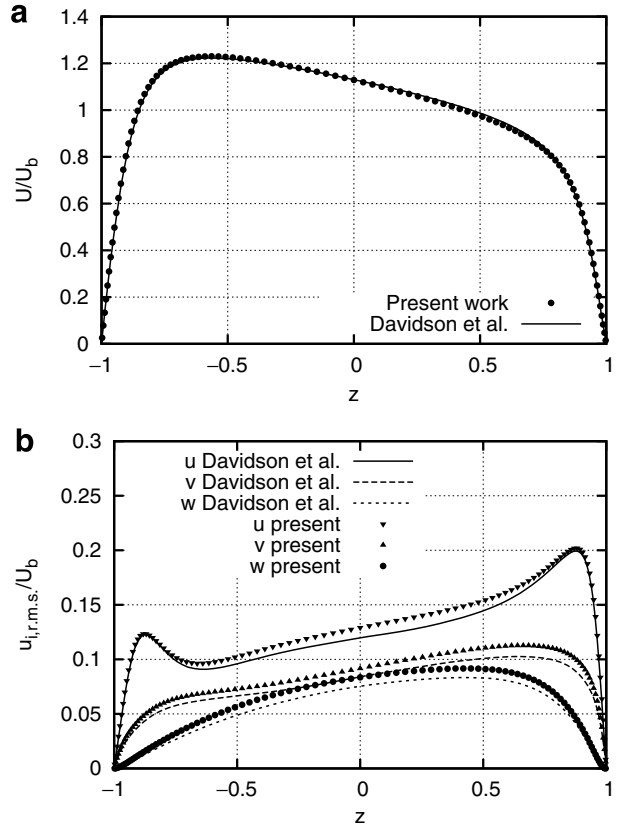

Fig. 7. Mean (a) and r.m.s. (b) velocity profiles.

Table 2
Mixed convection relevant quantities.

$\tau_{w,-\delta}$	$\tau_{w,\delta}$	U_b	T_b	$\langle u_\tau \rangle$	$-(\partial\overline{T}/\partial z)_w$	Re_b
0.68 (*0.71*)	0.40 (*0.42*)	9.1 (*9.8*)	0.42	0.74 (*0.75*)	2.42 (*2.31*)	2722

locations along the streamwise direction; near the inlet at $x/\delta = 6.0$, in the middle of the channel length at $x/\delta = 12.5$ and near the outlet at $x/\delta = 24.0$. The local friction velocities at the top and bottom walls have been used for the scaling of the profiles corresponding to the upper and lower half-width of the channel and shown in Fig. 8a. The fluctuations intensities at the same streamwise positions are shown in Fig. 8c. The profiles corresponding to the case A are included in these figures for comparison purposes. It is important to note that when the buoyancy is considered, symmetry with respect the channel centerline is lost and different friction velocities are obtained for the two walls.

Table 3 shows the non-dimensional averaged friction velocities and wall shear stresses at the top and bottom walls. It can be seen that the wall shear stress is larger at the top wall than at the bottom wall because of the deflection of the plume towards the top wall. It can be seen in Fig. 8a that the averaged velocity profile for $z < 0$ scaled with the local friction velocity at the bottom wall agrees with the isothermal velocity profile while near the top wall ($z > 0$), where buoyancy considerably affects the flow, the profile exhibits lower values of the mean velocity. In δ -scaled coordinates the mean velocity decreases in the center of the channel (the maximum value has drifted towards the top wall) while it increases near the top wall as shown in Fig. 8b.

The mean wall-normal velocity component is shown in Fig. 9a. The w-component has very small values compared with its r.m.s. (Fig. 9b). In the mean field the flow is moving upwards very slowly and consequently the variation of the u-component mean profile along the channel is also small. However, it is important to note how r.m.s. values for the u-component grow near the upper wall as the streamwise position is increased as shown in Fig. 8c. The fluctuation intensities of u and w are larger in the middle of the channel ($x/\delta = 12.5$) than close to the outlet ($x/\delta = 24.0$). A similar tendency can be observed in the mean w component. This can be explained considering that at $x/\delta = 12.5$ the plume is moving upwards to the top wall and its development is very intense. Close to the outlet ($x/\delta = 24.0$), the plume is attached to the upper wall and the mean vertical velocity w is lower as it can be seen in Fig. 9a.

To clarify this point, the mean temperature contours at three selected positions are shown in Fig. 10 (dimensions have been scaled). The mean temperature field identifies clearer the different stages of the buoyant plume along the channel. Close to the inlet, $x/\delta = 6.0$, buoyancy starts to deflect the plume towards the upper wall. At the middle of the channel, $x/\delta = 12.5$, buoyancy effects moves the plume upwards but it is not completely attached to the wall. Finally, at $x/\delta = 24.0$, the plume reaches the top wall and approaches to its developed regime.

The mean temperature profiles for the selected locations are shown in Fig. 11a. The typical Gaussian bell profile associated with the mean scalar concentration (without wall effects) can be seen here for locations close to the inlet but displaced to the top wall due to the buoyancy effect.

The profiles of the temperature fluctuation intensities (see Fig. 11b) show a similar tendency with respect to the centerline. Two peaks are present even for advanced locations but symmetry with respect to $z = 0$ is not found. Compared with case A, buoyancy affects the mean temperature profile by deflecting the plume towards the upper wall while reduces the maximum intensities and increases its width. In a similar way, the two peaks in the fluc-

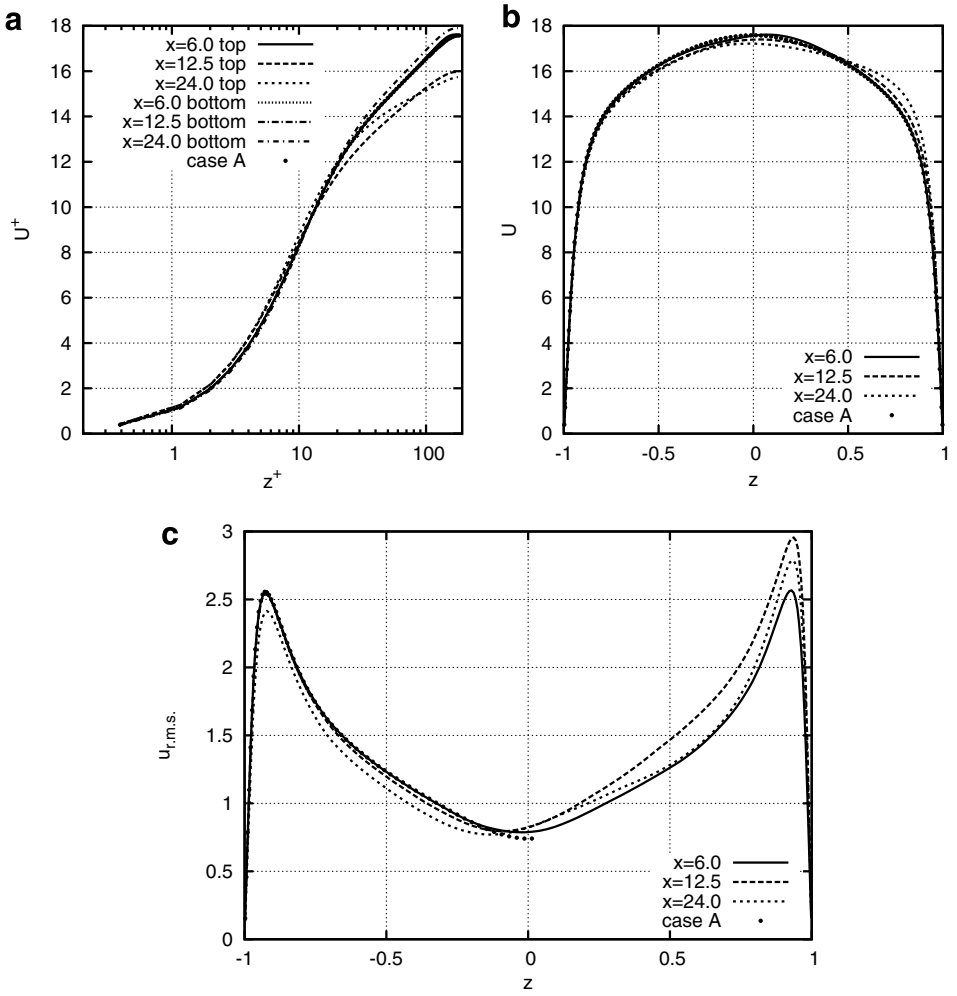

Fig. 8. Mean (a,b) and r.m.s. (c) u-component profiles.

Table 3
Averaged non-dimensional friction velocity and wall shear stress at the walls for case C.

Wall	$\langle u_\tau \rangle$	$\langle \tau_w \rangle$
Top	1.07	1.14
Bottom	0.99	0.97

tuation intensity profiles are not symmetrically distributed as they are in case A. In the upper zone of the plume the r.m.s. values are of the same order of magnitude as in case A while they decrease in the lower region. At $x/\delta = 12.5$ the behavior of the r.m.s. is similar but at $x/\delta = 24.0$ the r.m.s. values are higher in the lower part of the plume. This can be explained by the damping effect of the wall on the turbulence intensity.

4.3.2. Time averaged momentum and thermal energy budgets

In order to study the effect of the dispersion of the buoyant plume on the flow at different streamwise positions we analyzed the contribution of the different terms of the time averaged x and z-momentum equations as well as the heat transport equation.

In case C, the buoyancy acts in the wall-normal direction and only the spanwise direction remains as homogeneous. This implies that the dynamic field in this case is not fully developed. The time averaged x-momentum, z-momentum and heat equations can be written, respectively, as:

$$0 = \underbrace{-\frac{\partial UU}{\partial x}}_{1} \underbrace{-\frac{\partial WU}{\partial z}}_{2} \underbrace{+1-\frac{\partial P}{\partial x}}_{3} \underbrace{+\frac{1}{Re_\tau}\frac{\partial^2 U}{\partial x^2}}_{4} \underbrace{+\frac{1}{Re_\tau}\frac{\partial^2 U}{\partial z^2}}_{5} \underbrace{-\frac{\partial}{\partial x}(\overline{u'u'})}_{6} \underbrace{-\frac{\partial}{\partial z}(\overline{u'w'})}_{7} \tag{7}$$

$$0 = \underbrace{-\frac{\partial UW}{\partial x}}_{1} \underbrace{-\frac{\partial WW}{\partial z}}_{2} \underbrace{-\frac{\partial P}{\partial z}}_{3} \underbrace{+\frac{1}{Re_\tau}\frac{\partial^2 W}{\partial x^2}}_{4} \underbrace{+\frac{1}{Re_\tau}\frac{\partial^2 W}{\partial z^2}}_{5} \underbrace{-\frac{\partial}{\partial x}(\overline{w'u'})}_{6} \underbrace{-\frac{\partial}{\partial z}(\overline{w'w'})}_{7} \underbrace{+\frac{Gr}{8Re_\tau^2}(\overline{T}-T_{ref})}_{8} \tag{8}$$

$$0 = \underbrace{-\frac{\partial U\overline{T}}{\partial x}}_{1} \underbrace{-\frac{\partial W\overline{T}}{\partial z}}_{2} \underbrace{+\frac{1}{Re_\tau Pr}\frac{\partial^2 \overline{T}}{\partial x^2}}_{3} \underbrace{+\frac{1}{Re_\tau Pr}\frac{\partial^2 \overline{T}}{\partial z^2}}_{4} \underbrace{-\frac{\partial}{\partial x}(\overline{T'u'})}_{5} \underbrace{-\frac{\partial}{\partial z}(\overline{T'w'})}_{6} \tag{9}$$

Note that the second term in the pressure term (tagged 3) in Eq. (7) stands for the non-developed contribution to the pressure gradient. The numeration appearing at the bottom of Eqs. (7)–(9) is used in Figs. 12–20 to identify the different terms of the balances.

Figs. 12–20 show the profiles of the different terms of the time averaged x-momentum, z-momentum and heat transport Eqs. (7)–(9), respectively. Figs. 12–14 show the terms of the x-momentum

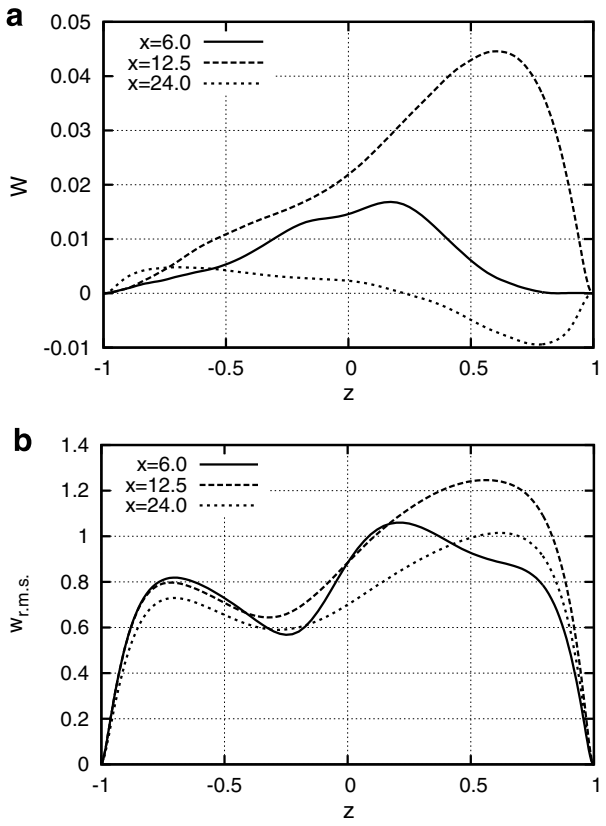

Fig. 9. Mean (a) and r.m.s. (b) w-component profiles.

equation at the streamwise positions $x/\delta = 6.0$, $x/\delta = 12.5$ and $x/\delta = 24.0$, respectively. The number in the brace labels of these figures identifies the different terms of Eq. (7).

Near the inlet, at $x/\delta = 6.0$ (Fig. 12), the pressure gradient is balanced by the wall-normal turbulent terms and the streamwise and wall-normal convection in the central region of the channel. The wall-normal turbulent term is the only one that balances the pressure gradient term in the fully developed case without buoyancy (case A). However, in the case C, the flow is not developed: the streamwise velocity gradient and the mean wall-normal velocity component are not zero and the convective terms exhibit significant values. The streamwise convective contribution is negative close to the upper wall where flow increases its velocity and positive for the lower zone where the flow decelerates. The wall-normal contribution behaves in the opposite way. While in the central region of the channel all the significant contributions have similar values in magnitude, near both walls, the wall-normal diffusion and the wall-normal turbulent contributions become the more important terms.

At $x/\delta = 12.5$ (Fig. 13), the situation is similar to that corresponding to $x/\delta = 6.0$. However, the wall-normal diffusion and the wall-normal turbulent flux increase in magnitude close to the top wall. Furthermore, in the upper region the contributions of the convective terms in the streamwise and wall-normal directions increase because of the plume deflection. As it was seen for the mean velocity and r.m.s. profiles, at this position the plume development is very intense. The streamwise velocity gradient and the wall-normal velocity component increase with respect to the $x/\delta = 6.0$ location.

At $x/\delta = 24.0$ (Fig. 14), the plume reaches the upper wall and the contribution of the convective terms decreases but is significant. The two main contributions in the near wall region (the wall-normal diffusion and the wall-normal turbulent flux) are similar to those found at $x/\delta = 6.0$ but their magnitudes are increased near the top wall and decreased slightly near the bottom one.

Figs. 15–17 show the contribution of the terms of the time averaged z-momentum equation. The number in the labels of these figures identifies the different terms of Eq. (8). The main terms of the budget are the pressure gradient, the wall-normal turbulent flux and the buoyancy while the convective and diffusive terms in the normal and streamwise directions do not contribute significantly. Note that the mean positive value of w is small and the buoyancy term is proportional to the mean temperature profile. The plume drifts towards the top wall as the position in the streamwise direction is increased and the maximum of the buoyancy term profile moves upwards according to this. At $x/\delta = 6.0$ (Fig. 15) the plume deflection is not important and the buoyancy term has a maximum close to the center of the channel ($z = 0$). The pressure gradient and the turbulent contributions are significant in the channel center region where they balance the buoyancy term. The plume is deflected only slightly so that near the walls the buoyancy term is not important and only the wall-normal turbulent and diffusive terms are significant.

At $x/\delta = 12.5$ (Fig. 16) the plume has been deflected towards the top wall so the buoyancy contribution becomes significant in the upper region of the channel with a maximum value that drifted upwards. Consequently, the pressure gradient and the turbulent contributions are increased in magnitude near the top wall. On the other hand, close to $z = 0$ the buoyancy magnitude is decreased due to the plume vertical dispersion and the pressure gradient and the turbulent contributions are decreased accordingly. Close to the bottom wall, where the buoyancy is not significant, the budget for the time averaged contributions resembles that found at $x/\delta = 6$.

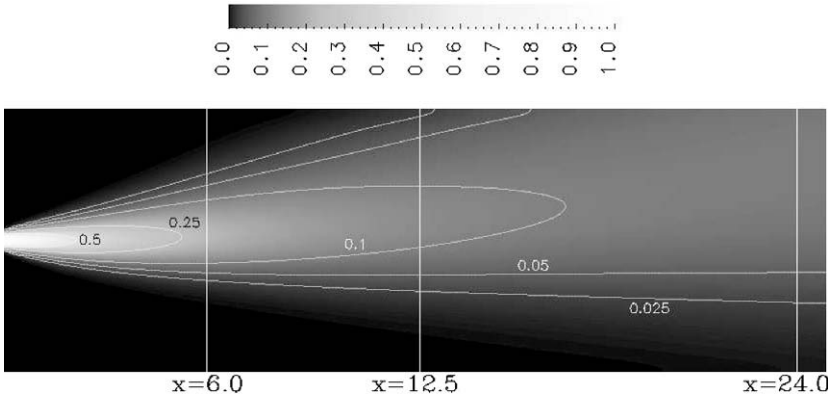

Fig. 10. Mean temperature field for case C.

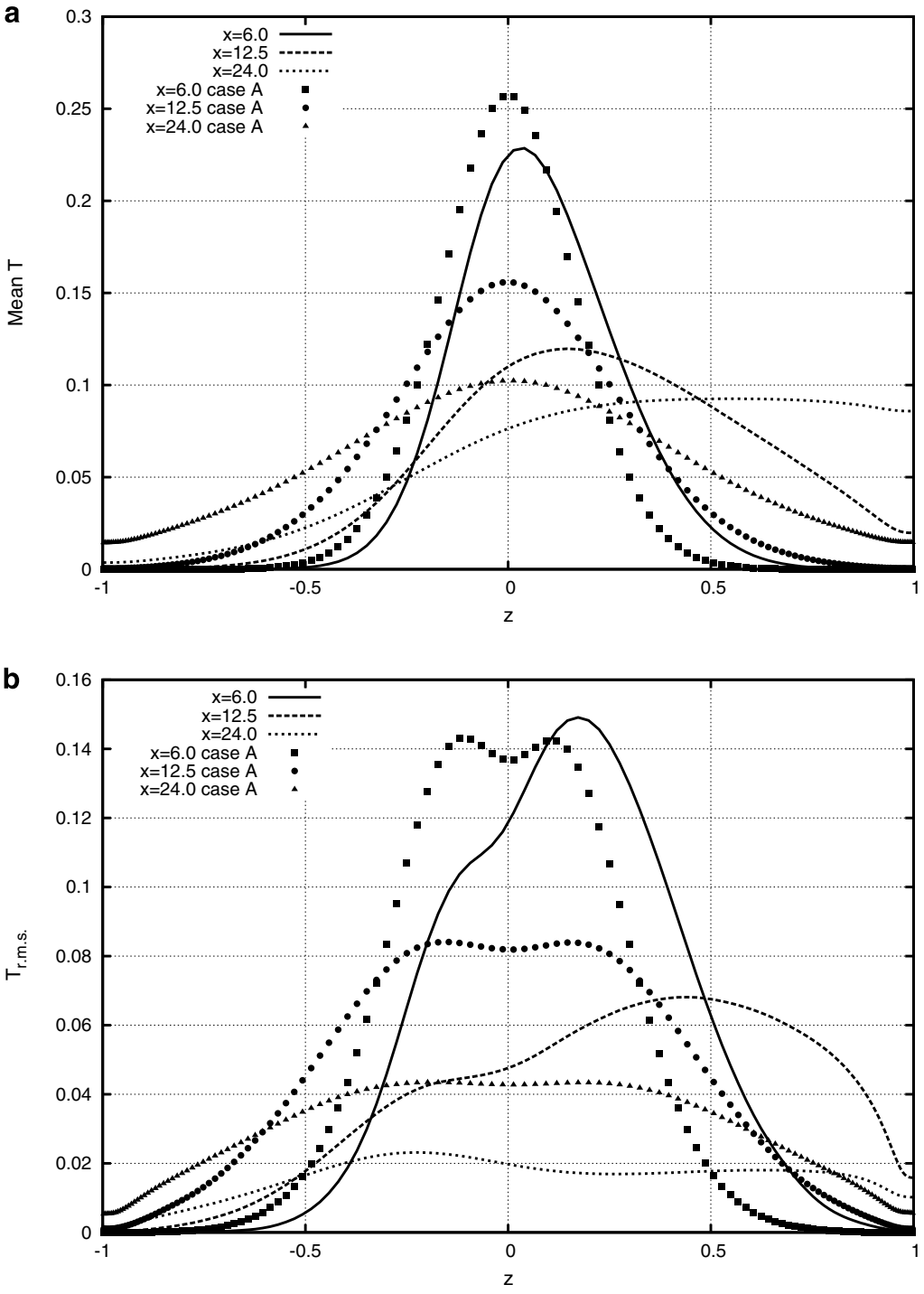

Fig. 11. Mean (a) and r.m.s. (b) temperature profiles.

Close to the outlet, at $x/\delta = 24.0$ (Fig. 17), the plume is attached to the top wall and its development is not as intense as that found for $x/\delta = 12.5$. The buoyancy term profile, proportional to the mean temperature, becomes smoother and shows a maximum closer to the top wall. Its magnitude on the top wall increases and the turbulent contribution is decreased while the pressure gradient term magnitude is similar to that found at $x/\delta = 12.5$. The situation close to the bottom wall, where the buoyancy is not significant, is similar to that found at $x/\delta = 6.0$ and $x/\delta = 12.5$.

Figs. 18–20 show the contribution of the different terms of the time averaged heat equation.

The contributions of the mean terms to the heat equation near the inlet are similar to those corresponding to the case A but shifted towards the top wall. The most important contributions are the streamwise convective and the wall-normal turbulent heat flux.

Close to the source, at $x/\delta = 6.0$ (Fig. 18), the two main contributions to the budget are very similar to those found in the case A (non-buoyant) in the central region of the channel. However, their magnitude increases close to the top wall and decreases close to the bottom one. This can be explained because of the plume deflection and the increase of the mean streamwise velocity near the top wall. The turbulent flux contribution in the upper zone of the

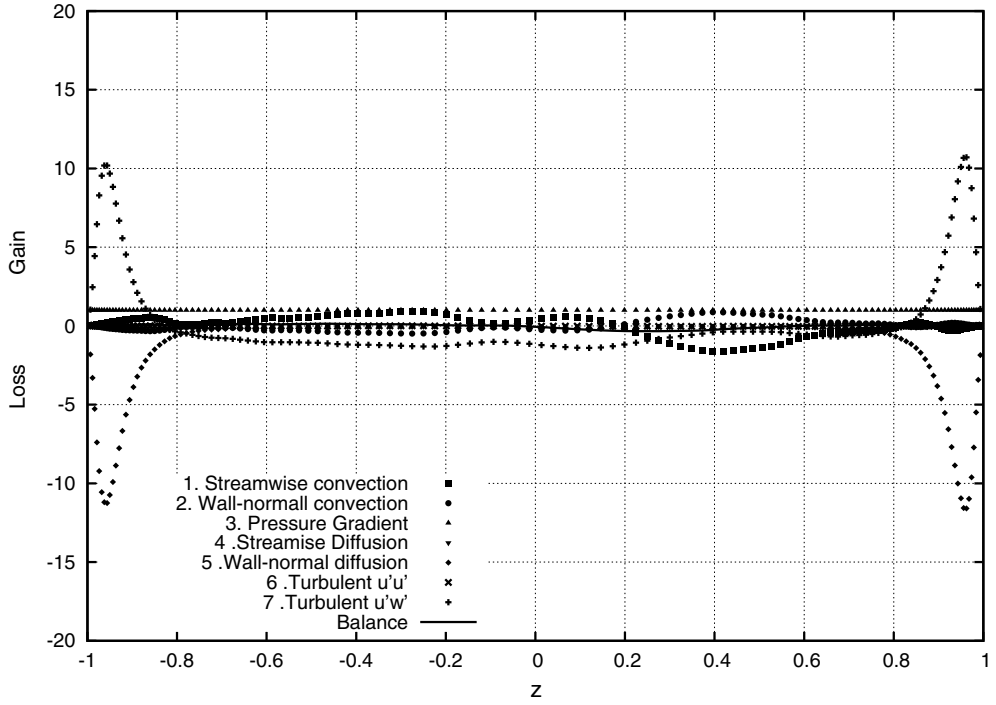

Fig. 12. Mean x-momentum transport balance at $x/\delta = 6.0$.

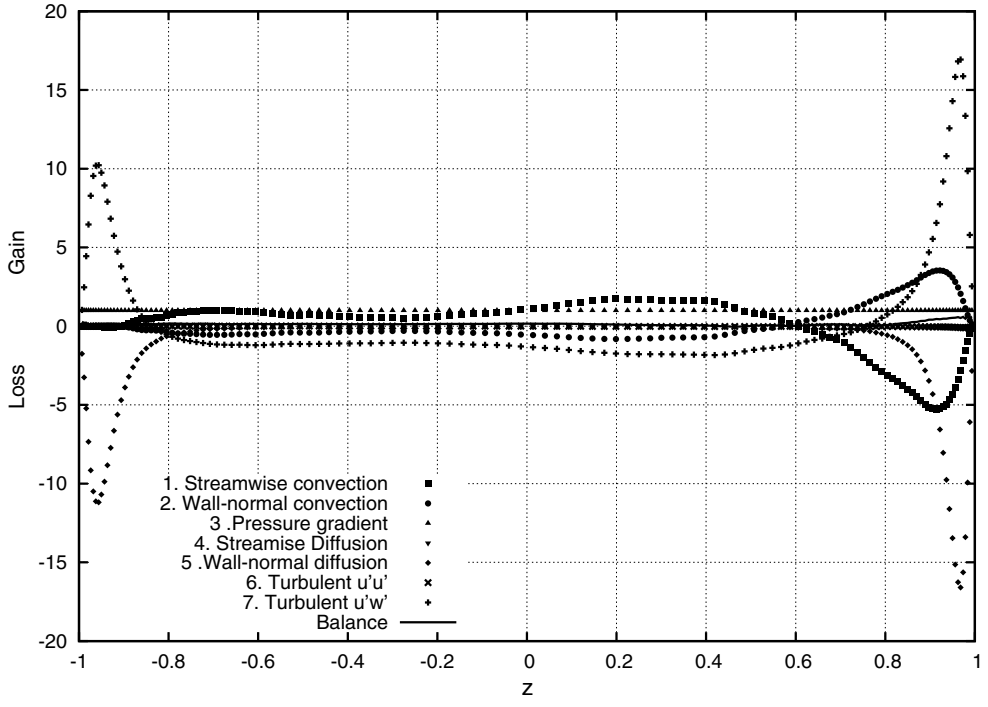

Fig. 13. Mean x-momentum transport balance at $x/\delta = 12.5$.

channel has to be larger than that at the lower one since this quantity is zero at the walls and its gradient in the wall-normal direction has to be larger in the upper zone. There is a small contribution of the wall-normal diffusion term specially significant in the central region of the channel. This contribution exists also in the non-buoyant case.

It should be noted that a conventional turbulent model based on the eddy diffusivity concept would fail in the prediction of the time averaged velocity and temperature profiles. For case C supression of the vertical turbulent fluxes below the plume centerline produced by buoyancy leads to negative values of the eddy conductivity in this region.

Once the plume reaches the top wall, at approximately $x/\delta = 12.5$ (Fig. 19), the absolute magnitude of the streamwise convective transport and the wall-normal turbulent flux in the region close to the top wall are as large as in the center of the

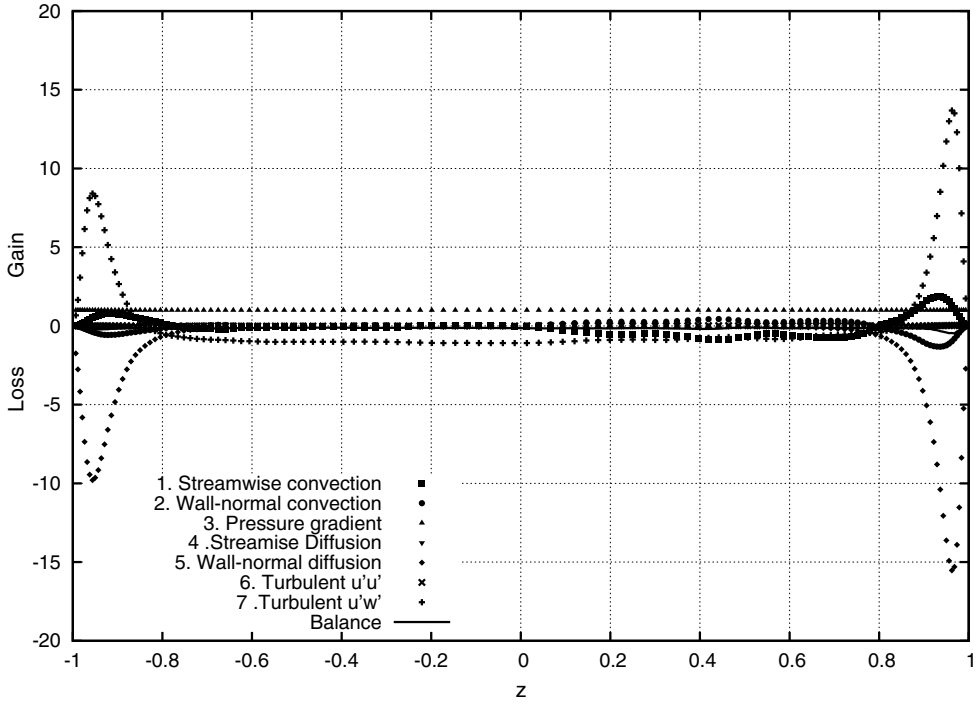

Fig. 14. Mean x-momentum transport balance at $x/\delta = 24.0$.

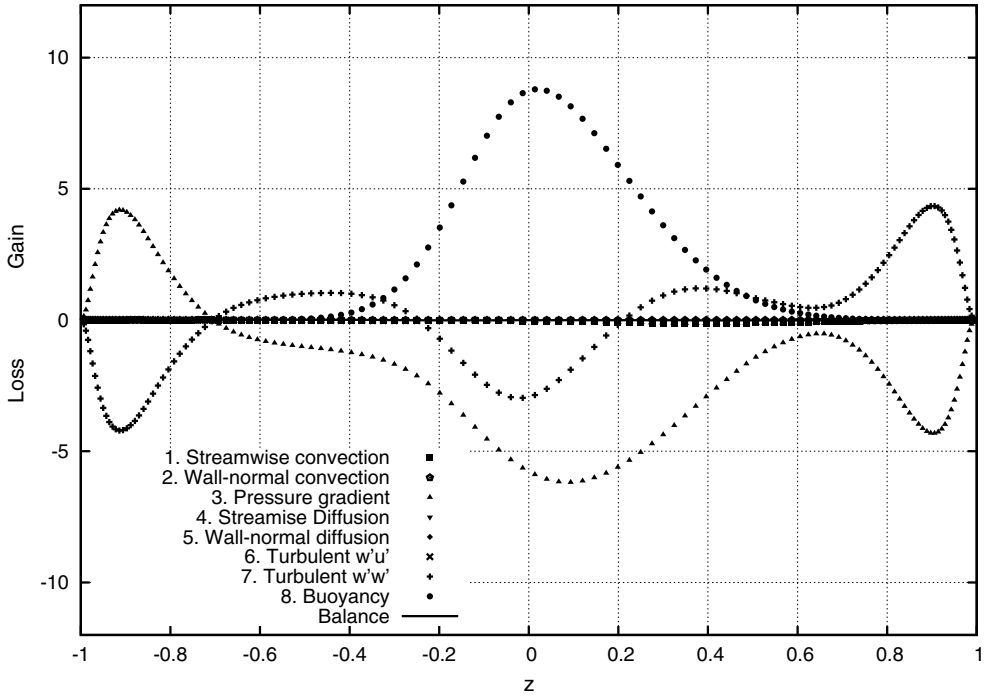

Fig. 15. Mean z-momentum transport balance at $x/\delta = 6.0$.

channel. As it is observed in the non-buoyant case, the wall-normal diffusive term becomes significant near the top wall. The plume does not reach the bottom wall, so this term is not significant there. It is important to note that the position at which the buoyant plume reaches the top wall is smaller than that for the non-buoyant case. The mean vertical velocity component has a small magnitude and consequently the wall-normal convective term becomes significant.

At $x/\delta = 24.0$ (Fig. 20), the magnitude of all the contributions has decreased. The streamwise convection and the wall-normal term are still the main contributions and they are similar in magnitude close to the top wall and in the central region of the channel. The plume has reached the top wall and the wall-normal diffusive term is still significant. Close to the top wall, the wall-normal convection is larger in magnitude than the diffusive term. Furthermore its sign close to the top wall has changed due to the sign change in the

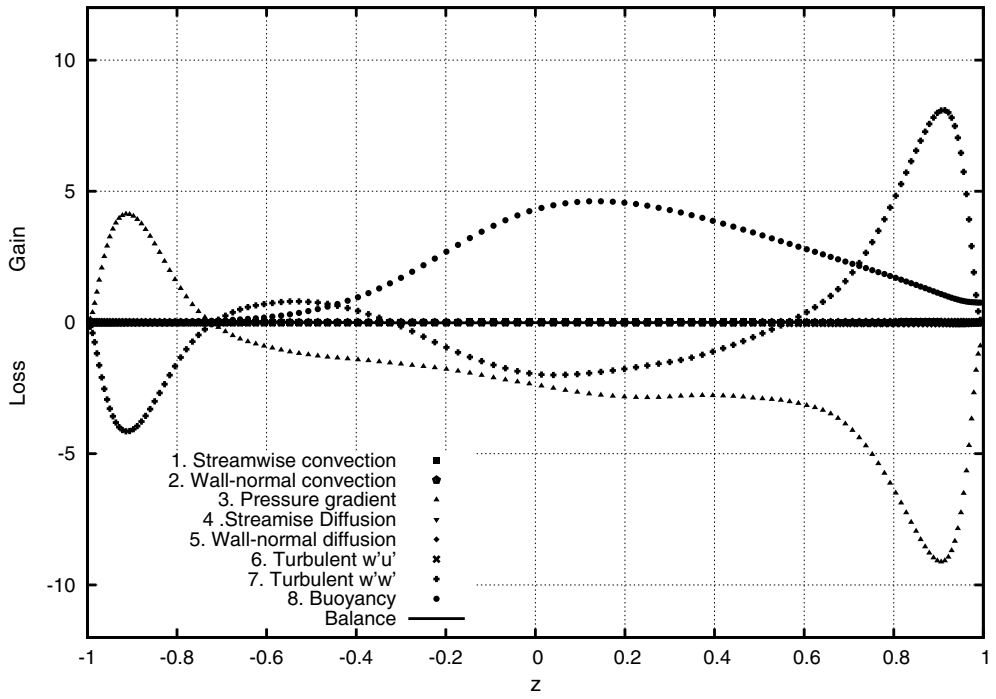

Fig. 16. Mean z-momentum transport balance at $x/\delta = 12.5$.

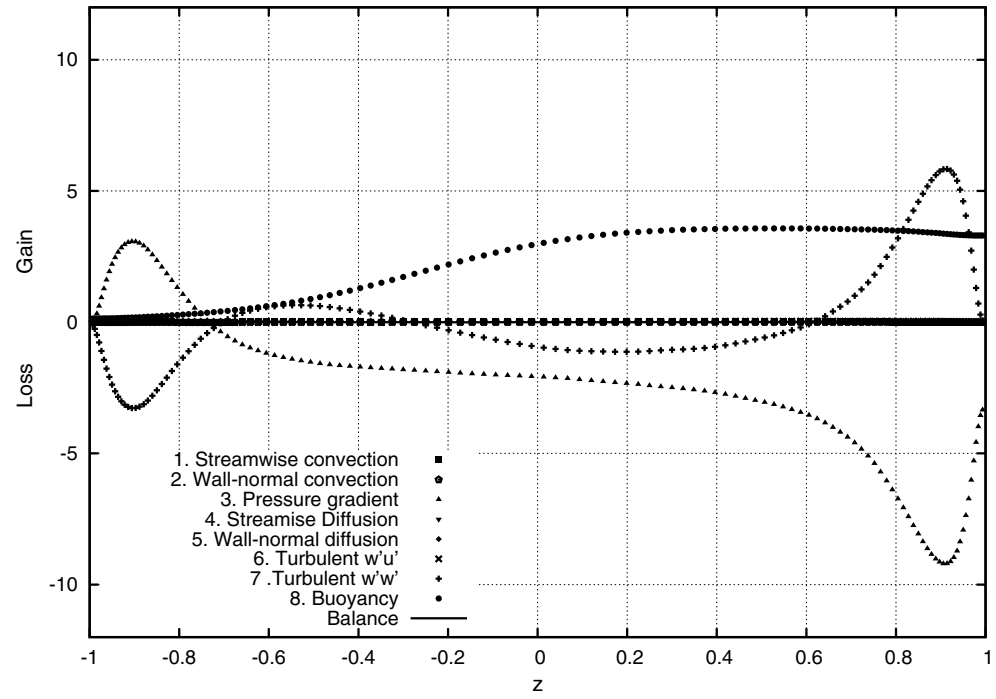

Fig. 17. Mean z-momentum transport balance at $x/\delta = 24.0$.

mean vertical velocity component (Fig. 9a). The streamwise turbulent term is also significant in the upper zone of the channel.

Due to the buoyancy forces acting along the wall-normal direction, case C is the only case considered with a non-fully developed dynamic field. Along the streamwise direction the pressure forces resulting from the mean pressure gradient are balanced by friction at walls. For case C, the term corresponding to the non-developed mean pressure gradient along the streamwise direction may be different from zero because of the development of the plume (see term 3 in the Eq. (7) for a decomposition of the mean pressure gradient into a developed and a non-developed contributions). The values of this term are less than 7% of the mean pressure gradient. Therefore this evolution has to be reflected on the quantities related with the friction on walls. Fig. 21 shows the profiles of the local friction velocity on both walls along the streamwise direction.

When the plume reaches the top wall at $x \approx 16$, the shear stress and consequently its friction velocity, increase. The position for the

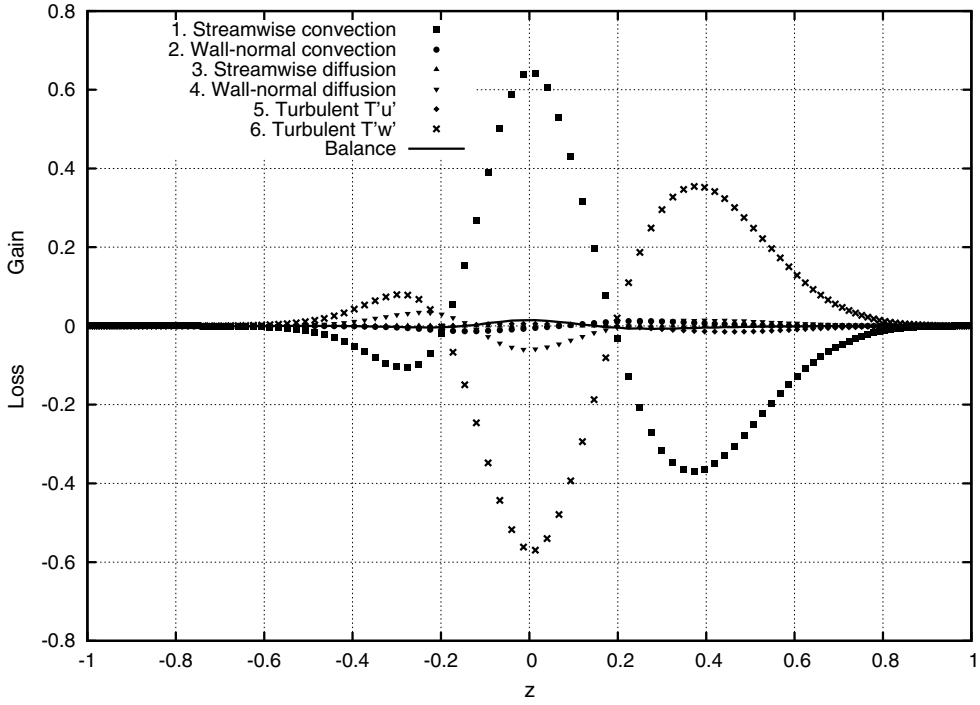

Fig. 18. Mean heat transport balance at $x/\delta = 6.0$.

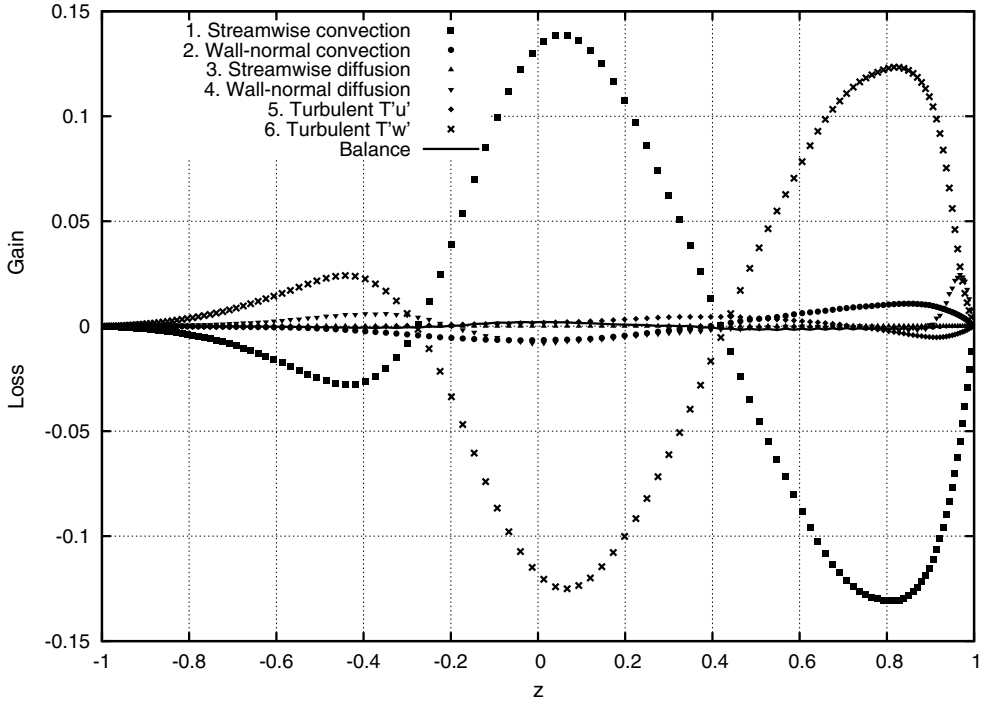

Fig. 19. Mean heat transport balance at $x/\delta = 12.5$.

maximum in this profile points out the location where the plume experiences the most intense evolution. After attaching the wall, the flow decelerates and the friction velocity decreases. On the other hand, on the lower wall the shear stress and the friction velocity decrease slightly. It can be seen that the size of the domain along the streamwise direction is not long enough for the flow to reach the fully developed state. At this stage, both shear stresses at the two walls would be constant and their mean would permit to obtain the corresponding friction velocity value that would balance the constant mean pressure gradient. The friction velocity can be expressed as:

$$u_\tau^* = \sqrt{\frac{1}{2Re_\tau}\left(\left.\frac{\partial U^*}{\partial z^*}\right|_b + \left.\frac{\partial U^*}{\partial z^*}\right|_t\right)} \tag{10}$$

where subscripts *b* and *t* stand for *bottom* and *top* walls.

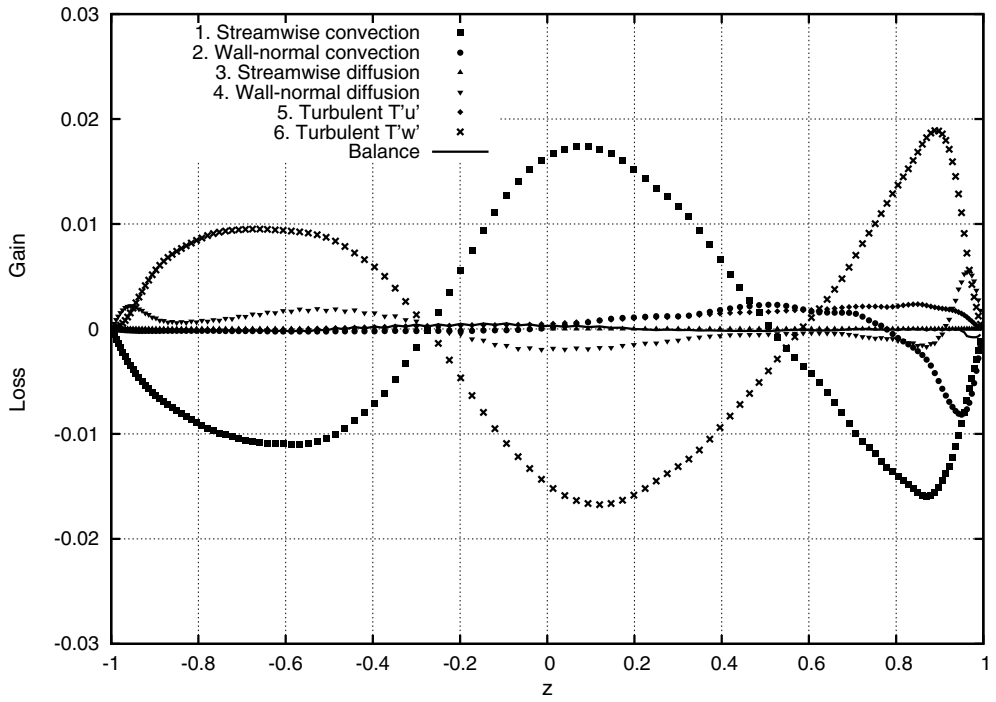

Fig. 20. Mean heat transport balance at $x/\delta = 24.0$.

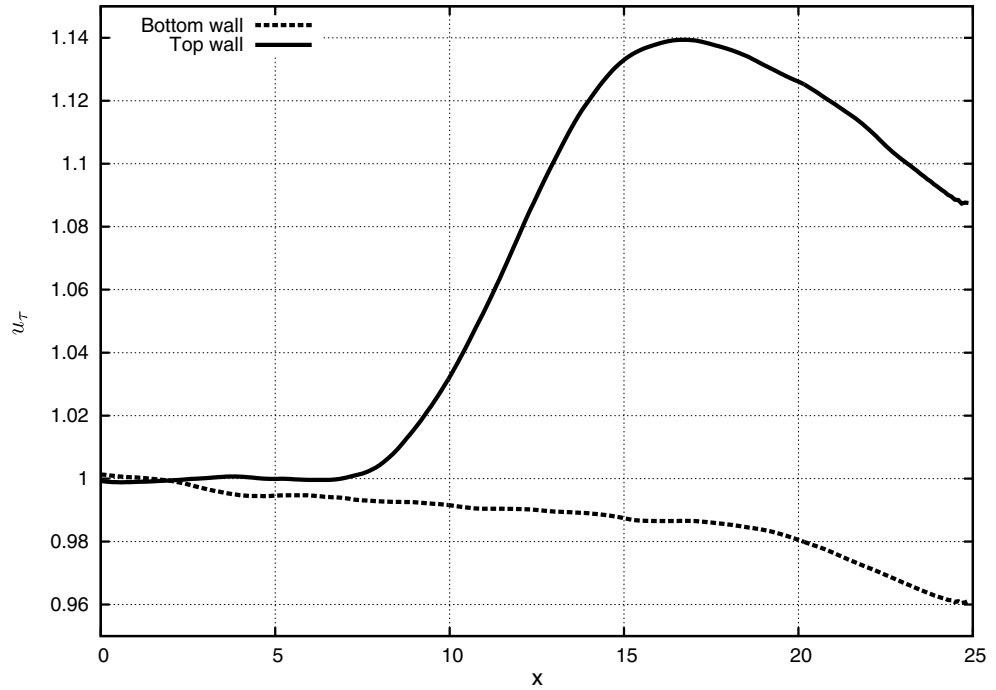

Fig. 21. Profile of u_τ on both walls.

4.3.3. Production terms of the turbulent kinetic energy

In order to obtain more insight from these results it may be convenient to study the transport for the turbulent kinetic energy $k = \frac{1}{2}\overline{u_i' u_i'}$. The k equation can be written as:

$$\frac{\partial}{\partial x_j}(U_j k) = \underbrace{-\overline{u_i' u_j'}\frac{\partial U_j}{\partial x_j}}_{1} - \frac{1}{2}\frac{\partial}{\partial x_j}(\overline{u_i' u_i' u_j'}) - \frac{\partial}{\partial x_j}(\overline{p' u_i'}) + \frac{1}{Re_\tau}\frac{\partial^2 k}{\partial x_j x_j} - \frac{1}{Re_\tau}\overline{\frac{\partial u_i'}{\partial x_j}\frac{\partial u_i'}{\partial x_j}} + \underbrace{\delta_{i3}\frac{Gr}{8Re_\tau}\overline{T' u_i'}}_{2} \qquad (11)$$

where the terms tagged 1 and 2 in the Eq. (11) stand for the production of turbulent kinetic energy and the buoyancy term, respectively.

The difference between the mean velocity field for the cases C and A is shown in Fig. 22 as a vector field. The difference of the turbulent kinetic energy k is shown as well with thin lines contours.

The contours with thick lines are used to show the difference between cases C and A for the production term of the turbulent kinetic energy (term 1 in Eq. 11) and the turbulent kinetic energy term due to buoyancy (term 2 in Eq. 11) in Fig. 22a and b, respec-

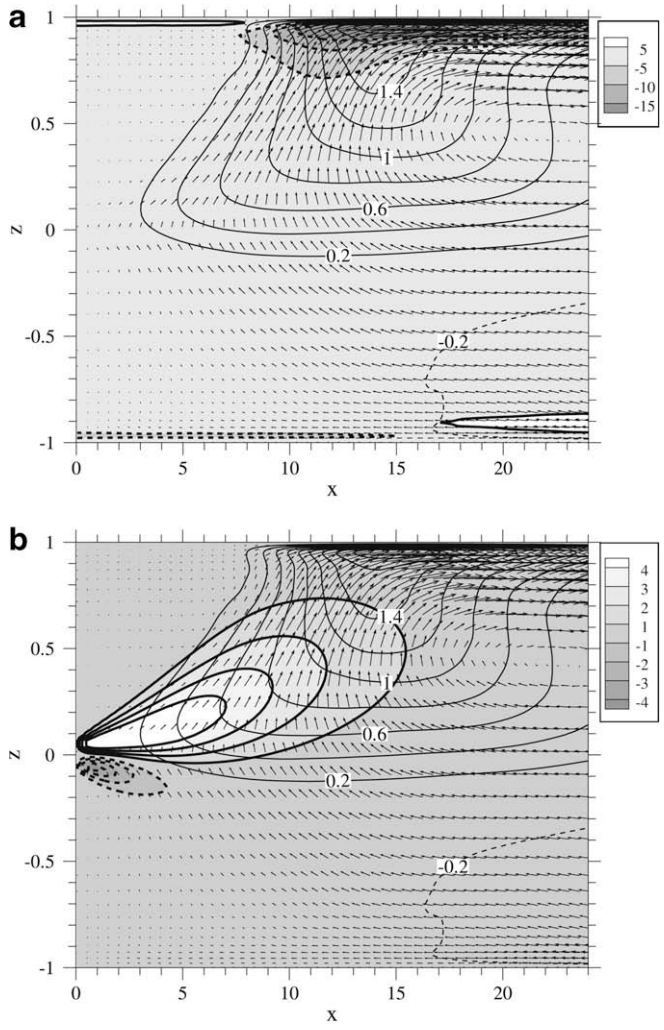

Fig. 22. (a) Thick dashed contours of the difference between the production term of the turbulent kinetic energy of cases C and A. (b) Thick line contours of the buoyancy term in the transport equation of the turbulent kinetic energy of case C. The difference of the time averaged velocity field and the difference of turbulent kinetic energy are shown in (a) and (b) with vectors and continuous thin contour lines respectively.

tively. The vertical dimension of the channel has been enlarged for clarity.

As it can be seen in the difference of the velocity field, the existence of a vertically centered line source releasing hot fluid at the inlet produces an upward fluid movement specially important in the top half of the channel. The region occupied by the rising plume exhibit the larger differences. As the plume approaches the top wall both the streamwise and the wall-normal velocity components increase due to the deflection produced by buoyancy. Once the plume has reached the top wall, the streamwise component is important speeding-up the flow near the top wall in comparison to case A. Near the outlet, the streamwise velocity component close to the top wall is larger but for $z < 0.4$ the streamwise velocity component at the outlet is lower than that found for case A. Lower u values for case C are also found in the entire lower half domain.

The difference of k attains maximum values close to the top wall and near the location $x/\delta \approx 16$. At this location the plume reaches the top wall and the friction velocity exhibits a maximum (see Fig. 21). The r.m.s. for both the streamwise and the wall-normal velocity components are higher close to this position than close to the channel outlet (see Figs. 8 and 9). The positive values for the difference of k between cases C and A are concentrated in the top half of the channel while negative values are located near the bottom wall and close to the outlet.

Taking into account that the spanwise direction y is homogeneous, the relevant contributions in the k production term can be written as:

$$\overline{u_i'u_j'}\frac{\partial U_i}{\partial x_j} = \underbrace{\overline{u'^2}\frac{\partial U}{\partial x}}_{1} + \underbrace{\overline{u'w'}\frac{\partial U}{\partial z}}_{2} + \underbrace{\overline{w'u'}\frac{\partial W}{\partial x}}_{3} + \underbrace{\overline{w'^2}\frac{\partial W}{\partial z}}_{4} \tag{12}$$

For the case A the turbulent kinetic energy production term profile is symmetric respect the channel mid centerline and its value is close to zero in most of the domain becoming significant close to the wall where the turbulent flux $\overline{u_i'u_j'}$ and the mean velocity gradient $\partial U_i/\partial x_j$ are larger. The most important contribution in the production of k (see Eq. 12) is the one tagged *2* while the contributions associated to the wall-normal velocity component gradient, tagged 3 and 4, are very small. The reason lies in the fact that the gradient of W both in the streamwise and wall-normal are much smaller than that for the streamwise velocity component.

The difference of the production term of k (see Fig. 22a) shows large negative values near the top wall while it remains close to zero in the most of the domain. In the region where the plume reaches the top wall the production of k is more important because of the increase of the mean velocity gradient and of $\overline{u'w'}$. The absolute maximum is again located at $x/\delta \approx 16$. Along the channel axial direction this component decreases and the magnitude of the k production decreases as well approaching to the values of case A for locations closer to the outlet. Fig. 22a shows that near the top wall at the inlet and near the bottom wall at the outlet there are two regions with positive sign. This means that in these two small regions the k production for case C is smaller than that obtained in case A.

The turbulent kinetic energy transport due to buoyancy (see Fig. 22b), which is proportional to the turbulent heat flux $\overline{T'w'}$, exhibits positive values near the top half of the plume. The dispersion process reduces the temperature gradients and consequently $\overline{T'w'}$ decreases as the plume advances along the channel. In this region the turbulent heat flux is positive because a positive fluctuation of w has associated an increase of temperature. This positive buoyancy contribution is associated with positive values for both streamwise and wall-normal velocity components. In the lower region of the channel and near the line source, it is possible to observe a negative buoyancy contribution region which is small compared with the positive one although as large as it in magnitude.

5. Conclusions

The mean and r.m.s. results for the fully developed channel flow at $Re_\tau = 180$ and $Pr = 0.71$ as well as the simulation of the mixed convection flow at $Re_\tau = 150$, $Pr = 0.71$ and $Gr = 9.6 \times 10^5$ show good agreement with previous DNS data.

The DNS of turbulent dispersion of a buoyant hot plume in an horizontal channel shows that the buoyancy force drifts the plume towards the top wall. This deflection produces positive values of the time averaged vertical velocity component which are small in comparison with its fluctuation intensity.

All the profiles of the mean streamwise velocity near the bottom wall at different x locations collapse on the universal profile using the wall coordinates scaling, otherwise maximum differences of 11% can be observed for profiles of the top half of the channel.

The comparison of the fluctuation intensities of the mean streamwise component with those corresponding to an isothermal

plane channel flow show larger values close to the top wall while slightly smaller values close to the bottom one.

At the location at which the plume reaches the top wall the local friction velocity has a maximum.

The local friction velocity on the bottom wall decreases monotonically as the streamwise position is increased.

The vertical plume dispersion is produced by the advective and diffusive transport mechanisms and it is enhanced in comparison with the non-buoyant case by the buoyancy effect.

The analysis of the contribution of the different terms of the streamwise and vertical momentum budgets revealed the mechanisms of the influence of the buoyancy term in the dispersion of the plume.

It has been found that the generation of a mean vertical advective transport of x-momentum by the buoyancy term produces an important redistribution of the contributions of the convective and turbulent transport terms. The change in the vertical momentum equation with respect to an isothermal plane channel flow are dominated by the streamwise and vertical evolution of the buoyancy term which is proportional to the temperature.

The budget of the heat transport equation shows that there is an overall increase of the vertical turbulent transport and of the streamwise advection near the top wall of the channel in comparison with the region near the bottom wall. The turbulent kinetic energy distribution along the streamwise direction shows maximum values at the top half of the channel and near the location at which the plume reaches the top wall. This increase of the turbulence intensity with respect to the isothermal plane channel flow is related to the augmentation of the buoyancy term near the centerline of the channel and by the mean shear production terms close to the top wall.

Acknowledgement

This study was financially supported by the Spanish Ministry of Science of Technology and FEDER under project DPI2006-0477.

References

[1] G.I. Taylor, Diffusion by continuous movements, Proc. Lond. Math. Soc. A 20 (1921) 196–212.
[2] G.I. Taylor, Statistical theory of turbulence IV-diffusion in a turbulent air stream, Proc. R. Soc. Lond. A 151 (1935) 465–478.
[3] M.S. Uberoi, S. Corrsin, Diffusion of Heat From A Line Source in Isotropic Turbulence, Technical Report , NASA Hampton VA Langley Research Center, 1952.
[4] A.A. Townsend, The diffusion behind a line source in homogeneous turbulence, Proc. R. Soc. Lond. A 224 (1954) 487.
[5] B.L. Sawford, J.R.C. Hunt, Effects of turbulence structure molecular diffusion and source size on scalar fluctuations in homogeneous turbulence, J. Fluid Mech. 165 (1986) 373–400.
[6] H. Stapountzis, B.L. Sawford, J.C.R. Hunt, R.E. Britter, Structure of the temperature field downwind of a line source in grid turbulence, J. Fluid Mech. 165 (1986) 401–424.
[7] M.S. Anand, S.B. Pope, Diffusion behind a line source in grid turbulence, in: 4th Symp on Turbulent Shear Flows, Springer, Karlsruhe, Germany, 1983, pp. 17.11–17.17.
[8] D. Livescu, F.A. Jaberi, C.K. Madnia, Passive-scalar wake behind a line source in grid turbulence, J. Fluid Mech. 416 (2000) 117–149.
[9] H. Stapountzis, R.E. Britter, Turbulent diffusion behind a heated line source in a nearly homogeneous turbulent shear flow, in: 6th Symp on Turbulent Shear Flows, Springer, Toulouse, France, 1987, pp. 9.2.1–9.2.6.
[10] U. Karnik, S. Tavoularis, Measurements of heat diffusion from a continuous line source in a uniformly sheared turbulent flow, J. Fluid Mech. 202 (1989) 233–261.
[11] M.K. Chung, N.H. Kyong, Measurement of turbulent dispersion behind a fine cylindrical heat source in a weakly sheared flow, J. Fluid Mech. 205 (1989) 171–193.
[12] J.D. Wilson, T.K. Flesch, S.E. Waters, Dispersion in sheared gaussian homogeneous turbulence, Boundary-Layer Met. 62 (1993) 281–290.
[13] M.S. Cho, M.K. Chung, Application of a reynolds stress/heat flux model to the turbulent thermal dispersion behind a line heat source in a uniformly sheared flow, Numer. Heat Transfer A-Appl. 32 (1997) 715–732.
[14] D.J. Shlien, S. Corrsin, Dispersion measurements in a turbulent boundary layer, Int. J. Heat Mass Transfer 19 (1976) 285–295.
[15] P. Paranthoen, A. Fouari, A. Dupont, J.C. Lecordier, Dispersion measurements in turbulent flows (boundary layer and plane jet), Int. J. Heat Mass Transfer 31 (1988) 153–165.
[16] J.E. Fackrell, A.G. Robins, Concentration fluctuations and fluxes in plumes from point sources in turbulent boundary layer, J. Fluid Mech. 117 (1982) 1–26.
[17] B.J. Legg, R.M. Raupach, P.A. Choppin, Experiments on scalar dispersion within a model plant canopy. Part iii: an elevated line source, Boundary-Layer Met. 35 (1986) 277–302.
[18] S. Veeravalli, Z. Warhaft, Thermal dispersion from a line source in a shearless turbulence mixing layer, J. Fluid Mech. 216 (1990) 35–70.
[19] B.M. Bara, D.J. Wilson, B.W. Zelt, Concentration fluctuations profiles from a water channel simulation of a ground-level release, Atmos. Environ. 26A (1992) 1053–1062.
[20] C. Tong, Z. Warhaft, Passive scalar dispersion and mixing in a turbulent jet, J. Fluid Mech. 292 (1995) 1–38.
[21] J.Y. Vincont, S. Simoens, M. Ayrault, J.M. Wallace, Passive scalar dispersion in a turbulent boundary layer form a line source at the wall and downstream of an obstacle, J. Fluid Mech. 424 (2000) 127–167.
[22] S.L. Lyons, T.J. Hanratty, J.B. McLaughlin, Direct numerical simulation of passive heat transfer in a turbulent channel flow, Int. J. Heat Mass Transfer 34 (1991) 1149–1161.
[23] D.V. Papavassiliou, T.J. Hanratty, Transport of a passive scalar in a turbulent channel flow, Int. J. Heat Mass Transfer 40 (1996) 1303–1311.
[24] Y. Na, T.J. Hanratty, Limiting behaviour of turbulent scalar transport close to a wall, Int. J. Heat Mass Transfer 43 (2000) 1749–1758.
[25] K. Kontomaris, T.J. Hanratty, Effect of molecular diffusivity on point source diffusion in the center of a numerically simulated turbulent channel flow, Int. J. Heat Mass Transfer 37 (1994) 1817–1828.
[26] Y. Mito, T.J. Hanratty, Lagrangian stochastic simulation of turbulent dispersion of heat markers in a channel flow, Int. J. Heat Mass Transfer 46 (2003) 1063–1073.
[27] P.H. Le, D.V. Papavassiliou, Turbulent dispersion from elevated line sources in channel and couette flow, AIChE J. 51 (2005) 2402–2414.
[28] G. Brethouwer, B.J. Boersma, M.B.J.M. Pourquie, F.T.M. Nieuwstadt, Direct numerical simulation of turbulent mixing of a passive scalar in a pipe flow, Eur. J. Mech. B/Fluids 18 (1999) 739–756.
[29] A.J. Vrieling, F.T.M. Nieuwstadt, Turbulent dispersion from nearby point sources - interference of the concentration stadistics, Atmos. Environ. 37 (2003) 4493–4506.
[30] R.A. Lavertu, L. Mydlarski, Scalar mixing from a concentrated source in turbulent channel flow, J. Fluid Mech. 528 (2005) 135–172.
[31] J. Kim, P. Moin, Transport of passive scalars in a turbulent channel flow, in: J.-C. A et al. (Eds.), Turbulent Shear Flows 6, Springer-Verlag, Berlin, 1989, pp. 85–96.
[32] D.V. Papavassiliou, Turbulent transport from continuous sources at the wall of a channel, Int. J. Heat Mass Transfer 45 (2002) 3571–3583.
[33] J.D. Li, R.W. Bilger, The diffusion of conserved and reactive scalars behind line sources in homogeneous turbulence, J. Fluid Mech. 318 (1996) 339–372.
[34] Z. Warhaft, The interference on thermal fields form line sources in grid turbulence, J. Fluid Mech. 144 (1984) 363–387.
[35] G. Brethouwer, F.T.M. Nieuwstadt, DNS of mixing and reaction of two species in a turbulent channel flow: A validation of the conditional moment closure, Flow Turbul. Combust. 66 (2001) 209–239.
[36] P.S. Bernard, A.L. Rovelstad, On the physical accuracy of the scalar transport modeling in inhomogeneous turbulence, Phys. Fluids 6 (1994) 3093–3108.
[37] Y. Wang, S. Komori, Application of a second-moment closure model to simulate the turbulent dispersion form an elevated source, Heat Mass Transfer 34 (1999) 429–436.
[38] I. Iliopoulos, T.J. Hanratty, Turbulent dispersion in a non-homogeneous field, J. Fluid Mech. 392 (1999) 45–71.
[39] J. Boussinesq, Théorie de l'Écolulement tourbillant, Mem. Présentés par Divers Savants Acad. Sci. Inst. 23 (1877) 45–50.
[40] A. Fabregat, Direct numerical simulation of turbulent dispersion of buoyant plumes in a pressure-driven channel flow, Master's thesis, Universitat Rovira i Virgili, Departament d'Enginyeria Mecànica, Tarragona, Spain, 2006.
[41] B. Koren, A Robust Upwind Discretization Method for Advection, Diffusion and Source Terms, Technical Report, Centrum voor Wiskunde en Informatica, 1993.
[42] D. Čuturić, Large-eddy simulation of turbulent channel flow significantly affected by buoyancy, Master's thesis, Chalmers University of Technology, Department of Thermo and Fluid Dynamics, Göteborg, Sweden, 2001.
[43] K. Iwamoto, Database of Fully Developed Channel Flow Tech Rep, The University of Tokyo, Berlin, 2002.
[44] B.L. Sawford, P.J. Sullivan, A simple representation of a developing contaminant concentration field, J. Fluid Mech. 289 (1995) 141–157.
[45] L. Davidson, D. Čuturić, S. Peng, DNS in plane vertical channel with without buoyancy, Turbul. Heat Mass Transfer 4 (2003) 401–408.